EPJ Web of Conferences **271**, 09003 (2022) https://doi.org/10.1051/epjconf/202227109003
HYP2022

Exploring the role of hyperons in high density matter in the Quark-Meson-Coupling model

Jirina R. Stone[1,2,*]

[1]Department of Physics and Astronomy, University of Tennessee, Knoxville, USA
[2]Department pf Physics (Astrophysics), University of Oxford, Oxford, UK

Abstract. Microscopic composition and properties of matter at super-saturation densities have been a subject of intense investigations for decades. Experimental and observational data and fundamental laws of physics indicate that heavy strange baryons and mesons are essential components of the matter. The Quark-Meson-Coupling-Model (QMC) is well suited for such a study. The model is based on interaction between quarks in individual baryons instead between the baryons as entities without internal structure. This approach significantly increases transparency and reduces the number of variable parameters of the model, thus offering deeper insight into the physics of high density hadronic matter. In this contribution, we review the effect of hyperons on neutron star (NS) properties, the speed of sound and the symmetry energy, both at zero and finite temperature. The QMC results are contrasted with the outcome of the traditional relativistic mean field DD2Y model. The (lack of) the so-called 'hyperon puzzle' in both models is discussed.

1 Introduction

Recent advances in detection and data analysis techniques in further exploration of hypernuclei and their properties, stimulated development in theoretical interpretation of the new data. More detailed information on Λ, $\Lambda\Lambda$ and, more recently, Ξ hypernuclei, and their excitations, as well as studies of the role of kaons in heavy-ion reactions is being obtained or is in an advanced planning stage. Theoretical interpretation and reliable prediction of the outcome of experiments is provided by several classes of models, based on various physical assumptions (e.g. realistic or density dependent NN potentials) used in different mathematical frameworks such as Bruckner G-matrix theory, chiral effective field theory and (non)relativistic mean-field models. As discussed, for example, by the author in [1], the main reason for existence of such a variety of theories is that the hadronic interactions in free space and, more importantly, in nuclear medium, is not known from first principles and has to be modelled. Models based on different physics and mathematical schemes yield similarly reasonable fit to data provided they have enough variable parameters, thus preventing identification of a model closest to true microscopy of hadronic interactions. Growing popularity of statistical approaches especially in astrophysical applications, taking advantage of multimessenger data, does not help in the quest for fundamentals of hadronic interactions. The consequence of this situation that we

*e-mail: jirina.stone@physics.ox.ac.uk

can obtain a reasonable reproduction of existing data but the predictive power of the models is limited, to say the least.

In this contribution we review the latest outcome of the Quark-Meson-Coupling-Model (QMC) for hyperonic matter. This model differs from the traditional relativistic mean-field models (RMF) in that that it is based on interaction between quarks in individual baryons instead between the baryons as entities without internal structure. Such approach leads to a significant reduction of variable parameters of the model as compared to traditional models, thus aiming to a well constraint parameter space. Most of the review is based on an extensive study of hadronic matter in the framework of the QMC-A variant of the model [2, 3], where more details can be found. Here we focus on effects of the hyperons on basic properties of cold and hot high-density matter and NS. The QMC results are contrasted with the outcome of the traditional RMF DD2Y model (labeled DD2 from now on) [2, 4].

2 The QMC model

2.1 The basics

The QMC is a phenomenological relativistic mean-field model of hadronic matter with a non-relativistic extension for finite systems, not discussed here. The key ideas of the model, here outlined for nucleons but valid for any baryons, are: (i) nuclear matter is a collection of quark bags with light quarks confined by attachment to a Y shaped colour string, moving in a non-perturbative QCD vacuum [5], (ii) quarks from different nucleons can come close enough to generate vacuum fluctuations, represented by scalar and vector meson fields - the origin of the nucleon-nucleon (NN) interaction in nuclear medium (see Fig. 1). The QMC

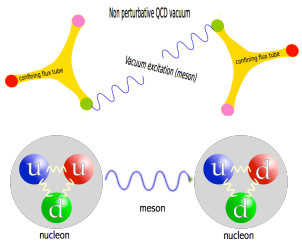

Figure 1: Mechanism of NN interaction in the QMC model (top) and in traditional RMF models which ignore the internal structure of the baryons (bottom). Adapted from Ref. [3] under Creative Commons Attribution License.

model was constructed by Guichon [6] and further developed in later years (see e.g. [7] and Refs. therein). The MIT bag is used as an effective realization of confinement for practical purposes. Although the bag strictly prevents quarks from crossing the boundary, it needs to be seen as an average representation of a more complex situation and the size and surface of the bag should not be given a deep physical meaning. The dynamical mass of the bag, immersed in a constant scalar σ field in a general case of the baryon octet (labeled by the index i for brevity) can be conveniently written as a function of the nucleon-meson coupling in free space $g_{\sigma N}$ (for details see Appendix in Ref. [8])

$$M_i(\sigma) = M_i - w_{\sigma i}\, g_{\sigma N}\, \sigma + \frac{d}{2}\tilde{w}_{\sigma i}(g_{\sigma N}\, \sigma)^2. \tag{1}$$

The coupling strength $g_{\sigma N}$ is a variable parameter of the model and is related to the quark-meson couplings as

$$g_{\sigma N} = 3g_{\sigma}^{q} \int_{Bag} d\vec{r}\, \bar{q}q(\vec{r}), \tag{2}$$

with q and $\bar{q}$ being the quark wavefunction and its conjugate.

The flavour dependence of the dynamical mass is controlled only by the weights $w_{\sigma i}$ and $\tilde{w_{\sigma i}}$ are fixed within the model (see Table 2 [7] and Appendix A in the Ref. [8]). The coefficient d in the third term in Equation 1, is known as the "scalar polarizability". This term is a natural consequence of the quark structure of the nucleon and is sufficient to lead to nuclear saturation. The scalar polarizability is related to the radius of the bag R_B as [7] $d = 0.0044 + 0.211 * R_B - 0.0357R_B^2$.

The total energy of a *classical* system of baryons at zero temperature, modeled as non-overlapping bags coupled to meson fields σ, ω and ρ is expressed as [7]

$$E_{QMC} = \sum_{i=1,...} \sqrt{P_i^2 + M_i^2(\sigma(\vec{R}_i))} + g_{\omega N}^{i}\omega(\vec{R}_i) + g_{\rho N}\vec{I}_i.\vec{B}(\vec{R}_i) + E_{\sigma} + E_{\omega,\rho}, \tag{3}$$

with $\vec{R}_i$ and $\vec{P}_i$ are the position and momentum of a baryon i and $\vec{I}$ is the isospin matrix. $\vec{B}$ stands here for the isovector ρ field to avoid a confusion with the baryon number density ρ [7]. The contributions of the quark-meson couplings are dependent on two more model variable parameters, $g_{\omega N} = 3g_{\omega}^{q}$ and $g_{\rho N} = g_{\rho}^{q}$. The meson contributions, E_{σ} and $E_{\omega,\rho}$ are obtained by solution, in the mean field approximation, of the meson field equations of motion. The model is then quantized by replacement $\vec{P}_i \rightarrow -i\vec{\nabla}_i$. The three variable parameters, conveniently written as effective coupling constants $G_{\sigma}=g_{\sigma N}^2/m_{\sigma}^2$, $G_{\omega}=g_{\omega N}^2/m_{\omega}^2$ and $G_{\rho}=g_{\rho N}^2/m_{\rho}^2$, are fitted to properties of nuclear matter at saturation. The fixed parameters of the model, used in this work, are the free ω and ρ meson masses, the σ mass equal to 700 MeV, the bag radius R_B = 1 fm, and σ self-interaction parameter, λ_3, which appears to be needed in finite nuclei [9], equal to zero.

2.2 Applications

Starting with the equation of state (EoS), shown in Fig. 2, we observe that there is a threshold density for appearance of hyperons at T=0; at non-zero temperature hyperons appear at all densities. The onset of hyperons at T=0 MeV, manifests itself by separation of the EoS for nucleon only (np) matter from the EoS for hyperonic matter (npY) which softens at densities above the threshold (left panel). At finite T, shown for β-equilibrated matter with entropy density S/A=2 k_B, labeled by NS(β), corresponding to temperatures between about 20 - 50 MeV [2], this kink disappears. As expected, the pressure increases with temperature, more markedly in the np matter. Comparing the results of the QMC and DD2 models at T=0 MeV, they differ significantly both in the hyperon onset density and hyperon content (see Fig. 2). The Λ hyperons appear in both models but at different thresholds; in addition, in the QMC model only both cascades are present. In the DD2 model, only the negatively charged Σ and Ξ hyperons appear.

Figure 3 illustrates the NS masses vs radius and central density of cold and hot stars, in comparison of the latest observational results. It demonstrates that neither model suffers from the so called 'hyperon puzzle' despite the sensitivity of the EoS to the hyperonic content. Naturally, the only np matter stars achieve higher maximum mass but the maximum mass of the npY stars are still within the observational limits. In the non-zero temperature case, shown for two proto-neutron stars scenarios, one with the fixed lepton fraction, S/A=1 k_B

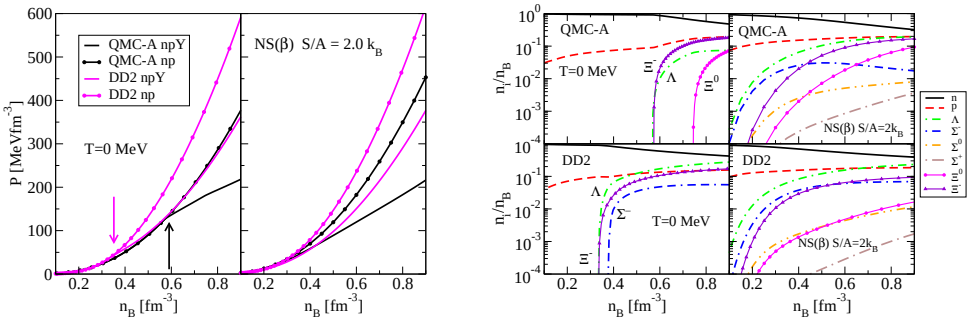

(a) *(b)*

Figure 2: (a) Equations of state of the QMC and DD2 models at T=0 MeV (left) and warm NS(β) matter (right), for full baryon octet (solid) and for only nucleons (dashed). (b) Relative population of nucleons and hyperons in units of the total baryon number density at T=0 MeV (left) and NS(β) matter (right). Only populations higher than 0.01% in the region of 0.1 - 1 fm^{-3} are shown (right). The figure is adapted from [2].

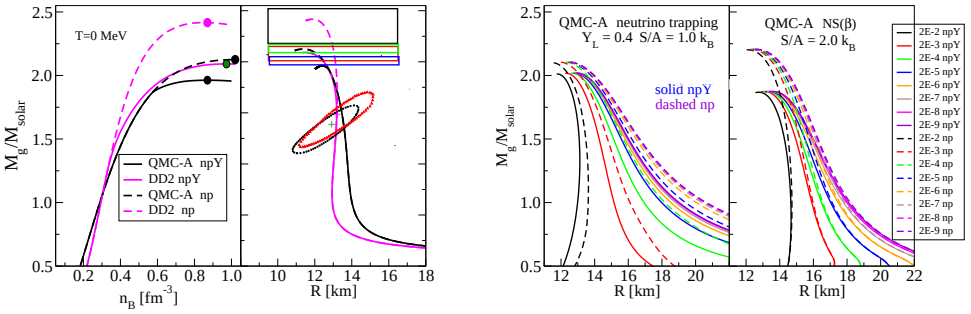

(a) *(b)*

Figure 3: (a) NS masses vs the central baryon density (left) and radius (right) computed with the QMC-A and DD2 models for hyperonic (solid line) and nucleonic (dashed) matter. Observational limits on the maximum mass configuration are illustrated by black dashed [10], green dot-double dash [11], red dot-single dash [12] and solid blue [13] rectangles. The NICER limits on the radius of a ∼1.4 $M_\odot$ PSR J0030-0451 [14] (magenta full triangles) and [15] (dark green full circles) are added for completeness. The coloured full circles in the left panel indicate the maximum mass. (b) Illustration of search for the surface of a hot star with fixed Y_p and S/A=1 k_B (left) and the for NS in β (right). The figure is adapted from [2].

and trapped neutrinos, and the other with the neutrinoless NS(β) matter, the maximum mass is somewhat higher, as expected. Note that at finite T the surface of the star is diffused and has to be determined by search for a close-to-zero surface pressure as a function of radius [2].

Finally, we show in Fig. 4 two other examples, not directly related, of applications of the models. The single-particle potentials of hyperons in high-density matter determine their ap-

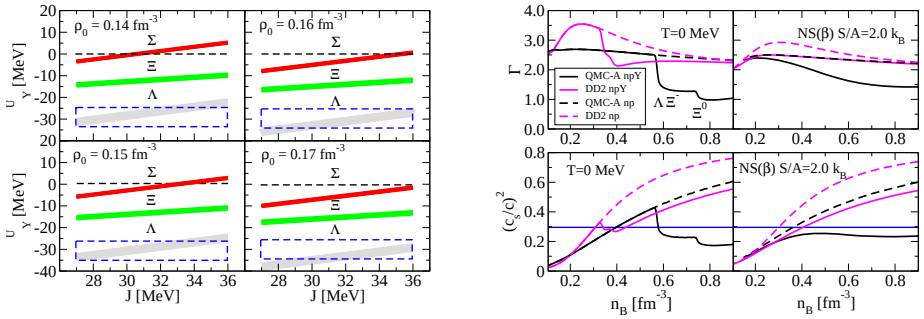

(a) *(b)*

Figure 4: (a) Single-particle potentials U_Λ (grey), U_Σ (red) and U_Ξ (green) as a function of the symmetry energy coefficient J for the saturation densities ρ_0 between 0.14 and 0.17 fm^{-3}. The filled width of the rectangles depicting the potentials represents the uncertainty due to the spread in the saturation energy E_0/A between -15.0 and -18 MeV. The dashed blue rectangle around U_Λ represents the region of experimental values reported in the literature. The horizontal black dashed line guides the eye to zero, dividing positive and negative values of U_Σ. No established experimental constraint on U_Ξ is available. Taken from Ref. [3] under Creative Commons Attribution License. (b) The adiabatic index Γ and the square of speed of sound in units of c for T=0 MeV (left top and bottom) and for NS(β) (top and bottom right). Predictions of the QMC-A model (black) and the DD2 model (green) are shown, both for npY (solid) and np (dashed) matter. The blue horizontal line indicates the conformal limit $(c_s/c)^2$ = 1/3. The figure is adopted from [2].

pearance in NS. These potentials are dependent on the nucleon-hyperon and hyperon-hyperon interactions, calculated within the QMC model, but treated as variable parameters in traditional RMF models. Specifically, the appearance of Σ hyperons in T=0 MeV models has been an issue for many years and both positive and negative U_Σ values have been considered [2, 3]. Here we show, in the left panel of Fig. 4, the relation of the potentials to saturation properties of nuclear matter as calculated in QMC-A. The positive U_Σ, consistent with the absence of Σ hyperons below ∼1 fm^{-3}, and unbound Σ hypernuclei, together with U_Λ being within a better known limit, places a strong constraint on the symmetry energy coefficient *J*. For this result being confirmed, data on U_Ξ are urgently needed, offering compelling support for experiments at JPARC.

In the right panel of Fig. 4 we show the density and temperature dependence of the adiabatic index Γ and the square of speed of sound as calculated in both QMC-A and DD2 models. Both quantities are directly related to the hyperonic content of the matter (see Fig. 2). The large drop in Γ at density 0.5-0.6 fm^{-3} for QMC-A takes place because the Λ and Ξ^- hyperons appear at almost the same density and the next drop is clearly related to appearance of the Ξ^0. The DD2 model predicts very close density thresholds for the Λ , Σ^- and Ξ^- hyperons, which can be associated with the large unresolved drop below 0.4 fm^{-3} (for more detail see [2]). At finite T, In the density dependence of Γ is smooth in both models, reflecting the absence of the thresholds, present in the T=0 MeV case. The speed of sound exhibits sensitivity to hyperon presence as well. In cold matter, $(c_s/c)^2$ decreases below the conformal limit with the onset of hyperons in the QMC-A model, but increases with density in DD2 (with a minimal glitch around 0.3 fm^{-3}). In warm matter, $(c_s/c)^2$ remains below the limit at all densities in hyperonic matter in QMC-A; in the DD2 model, it increases monotonically with density above the

conformal limit for densities higher than about 0.4 fm^{-3}. Naturally, there is no structure in density dependence of either Γ or $(c_s/c)^2$ in np matter.

3 Summary and outlook

In summary, we have explored the complex effects of hyperon presence in high-density matter in the cores of cold and warm NS. Starting with the EoS and the composition of the core, following through the NS gravitational mass vs radius and central energy density dependences, to the relation between of the hyperon single-particle potentials and nuclear matter saturation properties and to the adiabatic index and the speed of sound, we conclude that the hyperons play a multifaceted role in the physics of high density matter and NS. The QMC model is one of the possible avenues to finding answers to the problem of hyperonic interactions in medium. However, it is also a phenomenological model and does not provide a full answer to the microscopy of baryon interactions which is still waiting to be discovered.

References

[1] J.R. Stone, Universe **7**, 257 (2021)
[2] J.R. Stone, V. Dexheimer, P.A.M. Guichon, A.W. Thomas, S. Typel, MNRAS **502**, 3476 (2021)
[3] J.R. Stone, P.A.M. Guichon, A.W. Thomas, Frontiers in Astronomy and Space Sciences **9** (2022)
[4] S. Typel, G. Röpke, T. Klähn, D. Blaschke, H.H. Wolter, Physical Review C **81**, 015803 (2010)
[5] F. Bissey, F.G. Cao, A.R. Kitson, A.I. Signal, D.B. Leinweber, B.G. Lasscock, A.G. Williams, Physical Review D **76**, 114512 (2007)
[6] P.A.M. Guichon, Phys. Letts. B **200**, 235 (1988)
[7] P.A.M. Guichon, J.R. Stone, A.W. Thomas, Progress in Particle and Nuclear Physics **100**, 262 (2018), 1802.08368
[8] J. Rikovska-Stone, P.A.M. Guichon, H.H. Matevosyan, A.W. Thomas, Nucl. Phys. A **792**, 341 (2007), nucl-th/0611030
[9] K.L. Martinez, A.W. Thomas, J.R. Stone, P.A.M. Guichon, Physical Review C **100**, 024333 (2019)
[10] R.W. Romani, D. Kandel, A.V. Filippenko, T.G. Brink, W. Zheng, The Astrophysical Journal Letters **934**, L17 (2022)
[11] R.W. Romani, D. Kandel, A.V. Filippenko, T.G. Brink, W. Zheng, The Astrophysical Journal Letters **908**, L46 (2021)
[12] E. Fonseca, H.T. Cromartie, T.T. Pennucci, P.S. Ray, A.Y. Kirichenko, S.M. Ransom, P.B. Demorest, I.H. Stairs, Z. Arzoumanian, L. Guillemot et al., The Astrophysical Journal Letters **915**, L12 (2021)
[13] J. Antoniadis, P.C.C. Freire, N. Wex, T.M. Tauris, R.S. Lynch, M.H. van Kerkwijk, M. Kramer, C. Bassa, V.S. Dhillon, T. Driebe et al., Science **340** (2013)
[14] M.C. Miller, F.K. Lamb, A.J. Dittmann, S. Bogdanov, Z. Arzoumanian, K.C. Gendreau, S. Guillot, A.K. Harding, W.C.G. Ho, J.M. Lattimer et al., ApJ **887**, L24 (2019)
[15] T.E. Riley, A.L. Watts, S. Bogdanov, P.S. Ray, R.M. Ludlam, S. Guillot, Z. Arzoumanian, C.L. Baker, A.V. Bilous, D. Chakrabarty et al., ApJ **887**, L21 (2019)